International Symposium
On Turbulence and Shear Flow
Phenomena (TSFP-9)
June 30 - July 3, 2015 *Melbourne, Australia*

HYDRODYNAMIC STABILITY ANALYSIS OF SHEARED CONVECTIVE BOUNDARY LAYER FLOWS IN STRATIFIED ENVIRONMENTS

Y. Xiao, W. Lin, Y. He
College of Sccience, Technology and Engineering
James Cook University
Townsville, QLD 4811, Austriala
email: yuan.xiao@my.jcu.edu.au
email: wenxian.lin@jcu.edu.au
email: yinghe.he@jcu.edu.au

S. W. Armfield, M. P. Kirkpatrick
School of Aerospace, Mechanical and Mechatronic Engineering
The University of Sydney
NSW 2006, Australia
email: steven.armfield@sydney.edu.au
email: michael.kirkpatrick@sydney.edu.au

ABSTRACT

Hydrodynamic stability analysis is carried out on sheared convective boundary layer (SCBL) flow, in which both sheared stratified flow and thermally convective flow coexist. The linear unstable stratification for the thermal convective flow region is included in the Taylor-Goldstein equations in terms of an unstable factor J_b in parallel with a stable stratification factor J. New unstable regions corresponding to the thermally convective instability are found above the pure sheared stratified flow regions in the wavenumber $\tilde{\alpha}$ versus stratification factor J plane. As the stratification ratio J_b/J increases, the unstable regions of thermal convection gradually approach and dominate the shear stratified unstable regions. The transition from shear stratified unstable mode to thermal convection unstable mode is also observed in the temporal growth rate $\tilde{\sigma}$ versus J plane and in the $\tilde{\sigma}$ versus $\tilde{\alpha}$ plane. The eigenfunctions of buoyancy, vertical velocity and buoyancy flux perturbations for sheared stratified dominant mode, the transitional mode and the thermal convection dominant mode in SCBL flow configuration are also discussed.

INTRODUCTION

As a representative geographical flow, sheared stratified (SS) flow in which sheared flow motions occur in a stratified environment has received substantial studies in the past decades. However, in the geographical settings such as the planetary or oceanic boundary layers and engineering settings involving heat transfer from radiation or chemical reaction, the comparable thermally convective flows inevitably coexist with sheared stratified flow, together forming a complex flow configuration, namely the sheared convective boundary layer (SCBL). SCBL flows have significant importantce for environmental issues, such as the mixing process of pollutants in atmospheric boundary layers, the heat and mass transfer in the upper ocean, and the mixing in large scale water bodies such as reservoirs, lakes and estuaries. The SCBL flows in fire-induced smoke transportation will potentially increase the fire hazards by changing flow patterns.

As pure thermally convective flows and pure sheared stratified flows have independent unstable modes, *i.e.* , the Rayleigh-Benard instability and shear stratified instability (*e.g.* , the Kelvin-Helmholtz instability and Holmboe instability), the combination of the two basic flow configurations are expected to produce more interactive and complicated unstable modes and corresponding flow patterns. For instance, Raasch & Franke (2011) used high resolution numerical simulation to find the transitional behaviour from a spoke-shape flow pattern in pure thermal convection to a band-like flow pattern in sheared thermal convection. Yang *et al.* (2010) observed experimentally a unique flow pattern near the interface in fire induced SCBL. Most recently, Stewart *et al.* (2014) investigated the SCBL flows with two-dimensional direct numerical simulation and found that the Kelvin-Helmholtz instability and the Rayleigh-Benard instability coexist in some stratification conditions, where the presence of the penetrative convection modifies the original Kelvin-Helmholtz eddy structures. Their results also suggest that new unstable modes might occur in the SCBL flow settings, which motivates the current hydrodynamic stability analysis to examine the stability features of the SCBL flow.

This paper will study the hydrodynamics of SCBL flow by introducing an unstable stratification factor J_b into the Taylor-Goldstein equation that describes the hydrodynamics of shear stratified flow. This idea comes from the hydrodynamic study of two-layer thermal penetrative convective flows where a thermally convective region is capped

by a stable stratified layer. The difference between the current SCBL flow and such two-layer penetrative convection is whether horizontal shear flow is present. By solving modified Taylor-Goldstein equations for SCBL flows, the instability features of the SCBL, including temporal growth rate and spatial perturbation structures, will be investigated, after a brief introduction of the numerical methodology.

PERTURBATION EQUATIONS

Based on the Taylor-Goldstein equations for sheared stratified flow and by applying the Squire transformations as detailed in Drazin & Reid (2004), the following perturbation equations, written in matrix form, have been derived by the current study,

$$\tilde{\sigma}\begin{bmatrix}\nabla_s^2 & \\ & I\end{bmatrix}\begin{bmatrix}\hat{w}\\ \tilde{b}\end{bmatrix}=\begin{bmatrix}-i\tilde{\alpha}(U\nabla_s^2-U_{zz}) & \dfrac{\tilde{\alpha}^2}{Fr^2}\\ \tilde{N}^2 & -i\tilde{\alpha}U\end{bmatrix}\begin{bmatrix}\hat{w}\\ \tilde{b}\end{bmatrix} \quad (1)$$

where the subscript 'zz' denotes the second order differentiation with respect to z, ∇_s^2 is the Squire Laplacian operator defined as $\nabla_s^2 = D^2 - \tilde{\alpha}^2$, $D = \partial/\partial z$ is the differential operator for the perturbation properties, $\tilde{\alpha}$ is the Squire wavenumber, I is the identity matrix, $\tilde{\sigma}$ is the Squire temporal growth rate of the perturbations properties, $\hat{w}$ and $\tilde{b}$ ($\tilde{b} = \gamma\tilde{\theta}$) are the vertical component of the velocity perturbation and the Squire buoyancy, $\tilde{\theta}$ is the Squire temperature, γ is the thermal expansion coefficient, and $\tilde{N}^2$ ($\tilde{N}^2 = \gamma\tilde{\theta}_z$) is the local Squire buoyancy Brunt-Väisälä frequency. For sheared stratified flows, the sheared layer thickness, the velocity and temperature changes across the sheared/stratified layer are usually selected as the characteristic length scale L, velocity scale $\Delta u_{*,0}$ and temperature scale $\Delta\theta_{*,0}$, respectively. $Fr = \Delta u_{*,0}/\sqrt{gL}$ is the Froude number where g is the gravitational acceleration.

Hazel (1972) suggested that when the basic velocity and background stratification in the sheared/stratified layer are in the form of $\Delta u_{*,0} f(z_*)$ and $\Delta\theta_{*,0} f(z_*)$, where $f(z_*)$ is a hyperbolic function, and if $(\partial u/\partial z)|_{z=0} = 1$ and $(\partial\theta/\partial z)|_{z=0} = 1$, where $z = 0$ is the central line of the sheared/stratified layer, then the local Richardson number $Ri_g(z)$ is

$$Ri_g(z) = \frac{N_*^2(z_*)}{(\partial u_*/\partial z_*)^2} = J\frac{(\partial\theta/\partial z)}{(\partial u/\partial z)^2}, \quad (2)$$

in which $J = g\gamma\Delta\theta_{*,0}L/\Delta u_{*,0}^2 = (g\gamma\Delta\theta_{*,0}/L)(L/\Delta u_{*,0})^2$. Here the bulk temperature gradient $\Delta\theta_{*,0}/L$ within the sheared/stratified layer is extracted. In practical stability analysis, J plays as an effective substitiute for Ri_g.

The SCBL flow system in this study is shown in figure 1, where the convective flow region with unstably linear stratification and the length scale L_b occurs at the bottom of the sheared stratified flow region with smooth tangential stratification and the length scale L. As the temperature at the bottom boundary $\theta_{b,*}$ is larger than the temperature $\theta_{1,*}$ the flows are unstable at $z_* < L_b$. However, when $z_* > L_b$, the flows are stably stratified as $\Delta\theta_{0,*} = \theta_{2,*} - \theta_{1,*} > 0$. In the convective flow region the bulk temperature gradient is $G_b = -\Delta\theta_{b,*}/L_b$, where the negative sign indicates that the temperature decreases with increasing height. Correspondingly, the bulk temperature gradient for the stably stratified

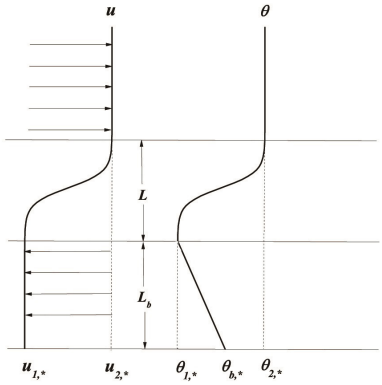

Figure 1. The SCBL flow configuration under consideration and the background velocity and stratification profiles.

layer is $G_s = \Delta\theta_{0,*}/L$, where the positive sign indicates that the temperature increases with increasing height.

In penetrative convection problems where a thermal convection region is capped by a stably stratified layer, Whitehead & Chen (1972) and Sun (1976) introduced a stability factor S by replacing the bulk temperature gradient in the Rayleigh number with the bulk temperature gradient in the top stably stratified layer. Inspired by this method, in the current SCBL flow, we replace the bulk temperature gradient G_s in J with G_b in the convective flow region $z < L_b$ and define the unstable stratification factor $J_{b,*}$ for SCBL flow as

$$J_b = -\frac{g\gamma\Delta\theta_{b,*}}{L_b}\left(\frac{L}{\Delta u_{*,0}}\right)^2 = g\gamma G_b\left(\frac{L}{\Delta u_{*,0}}\right)^2 = \frac{G_b}{G_s}J, \quad (3)$$

so that when $z > L_b$, $N_*^2 = J(\partial\theta/\partial z)$ and when $z < L_b$ $N_*^2 = J_b(\partial\theta/\partial z)$ in (2). It is noted that J_b and J have the opposite signs, indicating unstable and stable background stratification, respectively. Therefore, while solving (1), N_*^2 will become a piecewise function depending on if $z > L_b$ or $z < L_b$.

METHODOLOGY

The temporal mode of (1), where α is a real number and c is a complex number, is solved in this study. It should be noted that the real part of the temporal growth rate, $\tilde{\sigma} = i\tilde{\alpha}c$, of the perturbation is only determined by the imaginary part of the complex wave speed c, for the wavenumber $\tilde{\alpha}$ is fixed as a real number.

Matrix methods are used to solve the eigenvalue problems formed by discretising the perturbation equations (1) with uniform grid and using the second-order central difference scheme. The QZ algorithm developed by Moler & Stewart (1973), which is integrated in the LAPACK routine CGGEV, is used as the complex eigenvalue solver. The robustness of the QZ algorithm in hydrodynamic stability analysis has been demonstrated in some recent studies, such as Smyth *et al.* (2011), Liu *et al.* (2012), and Thorpe *et al.* (2013).

The boundary conditions $\hat{w} = \tilde{b} = 0$ are applied at both the top and the bottom boundaries. The dimensionless verti-

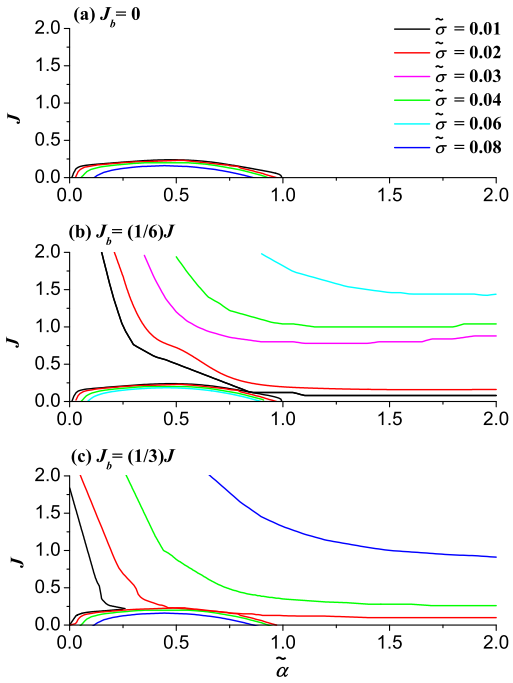

Figure 2. Contour plots of the real part of temporal growth rate $\tilde{\sigma}$ in the J versus Squire wavenumber $\tilde{\alpha}$ plane with (a) $J_b = 0$, (b)$J_b = (1/6)J$ and (c) $J_b = (1/3)J$. The magnitudes of $\tilde{\sigma}$ are denoted by curves in different colors.

cal coordinate z varies between -5 and 5, where z is made dimensionless by δ_s, giving the computational domain a size ten times that of δ_s, where the characteristic length δ_s is selected as one half of the sheared layer thickness. The length scale for the unstable stratified layer is $L_b = 3\delta_s$, which allows the unstable stratified layer to be adjacent to the central shear stratified layer. Based on (3), when $\Delta\theta_{*,0} = \Delta\theta_{*,b}$, $J_b = G_b = (1/3)J$. Thus, this study will change J_b in the way that J_b/J will be the factor of 1/3.

RESULTS

Growth Rate $\tilde{\sigma}$

Figure 2 shows the contours of the real part of the temporal growth rate $\tilde{\sigma}$ in the $J - \tilde{\alpha}$ plane for different unstable stratifications in terms of J_b. In figure 2(a) where $J_b = 0$ which represents that no convective flux exists, the unstable hemi-ellipse regions over $\tilde{\sigma} = 0 \sim 1$, in which the imaginary part of $\tilde{\sigma}$ (Im[$\tilde{\sigma}$]) is found to be zero, correspond to the stationary Kelvin-Helmholtz instability mode in SS flow as marked by 'SS'. The shapes of the KH mode regions are similar to the numerical results from Hazel (1972), where the critical stratification factor J_{cr} occurs at a corresponding critical wavenumber $\tilde{\alpha}_{cr} = 0.5$. As $J_b \neq 0$ when a convective flux is introduced, the other large unstable region where Im[$\tilde{\sigma}$]$\neq 0$ appears, as marked by 'RB' in figure 2(b) and figure 2(c). In figure 2(b), the 'RB' region interacts with the 'SS' region at $\tilde{\alpha} \approx 0.8$. In figure 2(c) when J_b is one thrid of J, the intersection points move to the small wavenumber range $\tilde{\alpha} \approx 0.25$ and the two contour curves of $\tilde{\alpha} = 0.2$ merge together at $\tilde{\alpha} = 0.45 \sim 0.8$. Inside this merging region, part of the $\tilde{\sigma} = 0.01$ contour, which was in the 'SS' region, is overwhelmed by the $\tilde{\sigma} = 0.02$ contour of the 'RB' region.

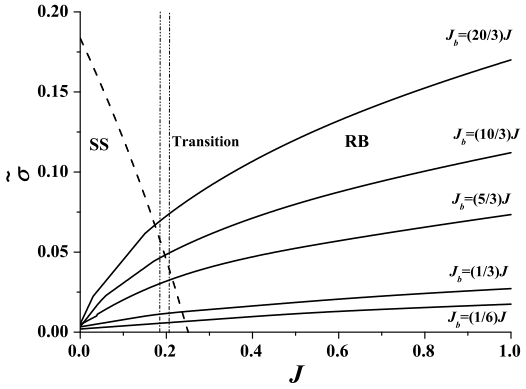

Figure 3. Calculated real part of the temporal growth rate $\tilde{\sigma}$ plotted against J at $\tilde{\alpha} = 0.5$. The results in the SS and RB unstable regiosn are denoted by the dashed and solid curves, respectively.

To further study the interactions between the two instability regions, figure 3 shows Re[$\tilde{\sigma}$] plotted against J at the critical wavenumber $\tilde{\alpha}_{cr} = 0.5$ for a series of J_b/J ratios. This figure can be considered as a vertical slice plot of figure 2 at $\tilde{\alpha} = 0.5$. The Im[$\tilde{\sigma}$]$= 0$ solutions for the 'SS' mode and the Im[$\tilde{\sigma}$]$\neq 0$ solutions for the 'RB' mode are denoted by dashed and solid curves, respectively. It is found that as different J_b/J are applied, the 'SS' curve retains its original shape at $J_b = 0$ although different 'RB' curves are obtained. Therefore, the 'SS' mode is independent of the 'RB' mode. As the 'SS' mode branch decreases quickly with increasing J and the 'RB' mode branch increases gradually with increasing J, the two branches intersect near the critical stratification factor $J = 0.25$ for SS flow. Near the intersection point, as Re[$\tilde{\sigma}$] in the 'RB' mode is comparable to that in the 'SS' mode, a narrow transition region where both 'SS' and 'RB' have equal influence is created. As J_b/J increases, the 'RB' mode curves gradually rise upwards and cap the 'SS' mode curves, thereby moving the intersection point upwards as well. As a result, some unstable regions which were in the 'SS' mode are replaced by the 'RB' mode, *e.g.* , $J = 0.20 \sim 0.25$ belong to the 'SS' region for $J_b < (10/3)J$ but belong to the 'RB' for $J_b > (10/3)J$.

Figure 4 shows the dispersion relations between Re[$\tilde{\sigma}$] and wavenumber $\tilde{\alpha}$ at $J = 0.2$. It can be considered as a horizontal slice plot of figure 2 at $J = 0.2$. Similar to the $J \sim \tilde{\sigma}$ plot in figure 3, the dispersion curves for the 'SS' and the 'RB' modes are represented by dashed and solid curves, respectively. Different from figure 3, two intersection points between the 'SS' mode dispersion curve and each 'RB' mode dispersion curve are found at small wavenumber range and large wavenumber range respectively, forming two transitional regions in the $\tilde{\alpha} \sim \tilde{\sigma}$ plane. As J_b increases, the 'RB' dispersion curves gradually rise based on their common origin point and move the two intersection points to larger Re[$\tilde{\sigma}$]. Consequently, more and more the 'SS' mode dispersion curve is dominated by the 'RB' mode dispersion curve, *e.g.* when $J_b = (8/3)J$ most parts of the 'SS' dispersion curve are covered by the 'RB' curves.

To quantify how the 'RB' mode gradually overwhelms

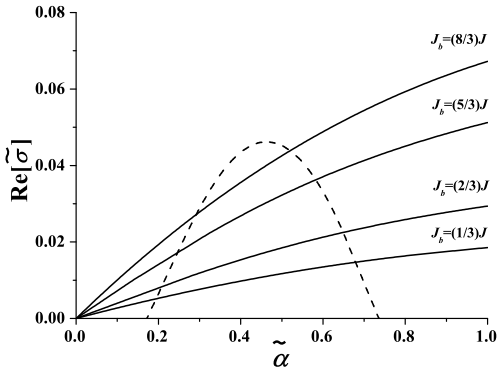

Figure 4. Calculated real part of the temporal growth rate $\tilde{\sigma}$ plotted against $\tilde{\alpha}$ at $J = 0.2$. The results in the SS and RB unstable regiosn are denoted by the dashed and solid curves, respectively.

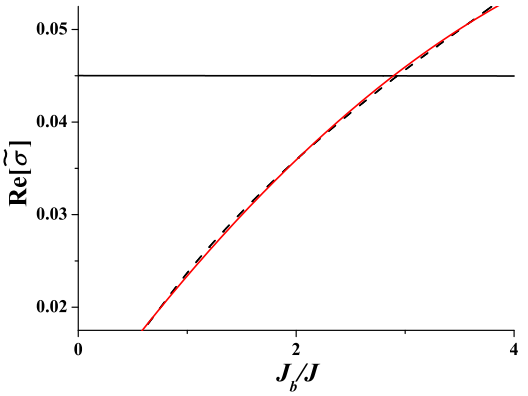

Figure 5. Calculated real part of the temporal growth rate $\tilde{\sigma}$ plotted against the stratification ratio J_b/J at $J = 0.2$ and $\tilde{\alpha} = 0.5$. The results in the SS and RB unstable regiosn are denoted by the dashed and solid curves, respectively. The parabolic correlation for the RB mode plot is denoted by the red solid curve.

the 'SS' mode as J_b increases, figure 5 shows Re$[\tilde{\sigma}]$ plotted against the stratification ratio J_b/J for both the 'SS' and the 'RB' modes at $\tilde{\alpha} = 0.5$ and $J = 0.2$. As both J and $\tilde{\alpha}$ are fixed, Re$[\tilde{\sigma}]$ for the 'SS' mode is constant at 0.045. On the other hand, Re$[\tilde{\sigma}]$ for the 'RB' mode increases with increasing J_b/J in a parabolic fashion, with the following correlation,

$$Re[\tilde{\sigma}]_{RB} = -0.00124(\frac{J_b}{J})^2 + 0.01625(\frac{J_b}{J}) + 0.00837, \quad (4)$$

where the subscript 'RB' indicates that the growth rate belongs to the 'RB' mode. It is noted that the 'RB' mode curve and the 'SS' mode curve intersect at $J_b/J = 3$, which indicates a critical transition stratification condition from the 'SS' mode to the 'RB' mode.

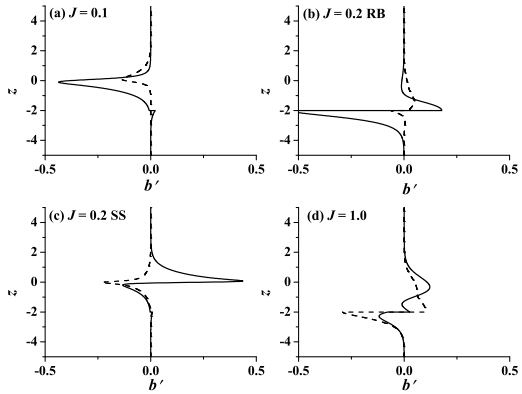

Figure 6. Calculated eigenfunctions of the buoyancy b' at $\tilde{\alpha} = 0.5$ with (a) J=0.1, (b) J=0.2 for the RB branch, (c) J=0.2 for the SS branch, and (d) J=1.0. The solid and dashed curves represent the amplitude and the phase, respectively.

Eigenfunctions

Based on figures 3 and 5, the eigenfunctions for buoyancy perturbation b', vertical velocity perturbation w' in (1) and their product, and buoyancy flux perturbation $B' = \theta' w'$ are studied at the critical wavenumber $\tilde{\alpha} = 0.5$ and stratification ratio $J_b/J = 3$, which is the intersection point found in figure 5. Three typical J values are selected at $J = 0.1$ where the 'SS' mode dominates, at $J = 0.2$ where the transition from the 'SS' mode to the 'RB' mode occurs, and at $J = 1.0$ where the 'RB' mode dominates. For $J = 0.2$, the Re$[\tilde{\sigma}]$ for the 'SS' and 'RB' modes are very close to each other, therefore the eigenfunctions for both modes are shown.

Figure 6 shows the calculated eigenfunctions for b' at $\tilde{\alpha}_{cr} = 0.5$ and $J_b/J = 3$ but with three typical J values as discussed above. The solid and the dashed curves represent the real and the imaginary parts of b', which correspond to the amplitude and the phase of b', respectively. At $J = 0.1$ where the 'SS' mode dominates, b' concentrated on the initial central shear/stratified layer, despite slight deviations of phase (dashed curve) due to weakly convective flow induced by the bottom unstable stratified layer. As J increases to 0.2, for the 'RB' mode as shown in figure 6(b), b' varies drastically near $z = -2$, which is the vertical height of the interface between the initial stable and unstable stratified layer. For the 'SS' mode as shown figure 6(c), the variation of b' remains at the central shear layer but its amplitude becomes positive compared to the negative one as shown in figure 6(a). As J increases to 1.0 where the 'RB' mode dominates, the absolute magnitude of the phase change (dashed curve) evolves to be larger than the amplitude change (solid curve) of b' at $z = -2$. Meanwhile, the amplitude variation along z in figure 6(d) keeps a similar profile to that shown in figure 6(b), and also shows a similar b' profile to that Sun (1976) where only penetrative convection occurs.

Figure 7 shows the calculated eigenfunctions for w' at $\tilde{\alpha}_{cr} = 0.5$ and $J_b/J = 3$ but with three typical J corresponding to figure 6. At $J = 0.1$, the central line of amplitude of w' is located slightly above the center of the initial shear layer ($z = 0$), as a result of weak convection flow due to a small J_b. At $J = 0.2$, the strong variation section of w' starts from the bottom of the domain for both the 'SS' and 'RB' modes.

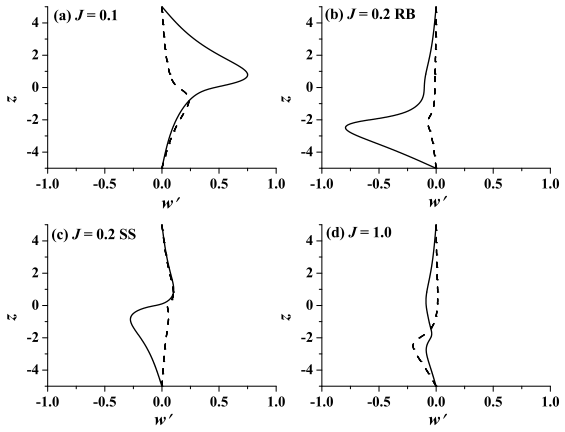

Figure 7. Calculated eigenfunctions of the vertical velocity perturbation b' at $\tilde{\alpha} = 0.5$ with (a) J=0.1, (b) J=0.2 for the RB branch, (c) J=0.2 for the SS branch, and (d) J=1.0. The solid and dashed curves represent the amplitude and the phase, respectively.

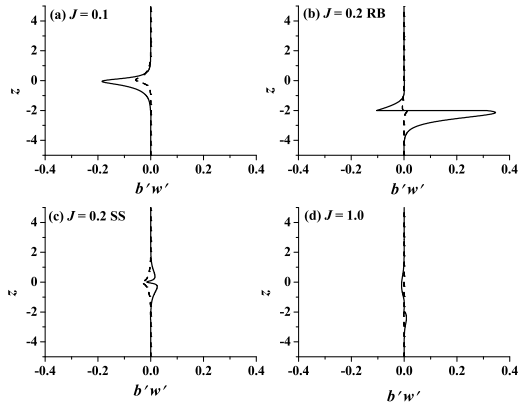

Figure 8. Calculated eigenfunctions of the buoyancy flux $b'w'$ at $\tilde{\alpha} = 0.5$ with (a) J=0.1, (b) J=0.2 for the RB branch, (c) J=0.2 for the SS branch, and (d) J=1.0. The solid and dashed curves represent the amplitude and the phase, respectively.

For the 'RB' mode, as shown in figure 6(b), the profile of the amplitude of w' changes remarkably at $z = -5 \sim -1$, indicating that most of w' originate from the bottom convective flow rather than from the initial shear layer which extends from $z = -1 \sim 1$. For the 'SS' mode as shown in figure 6(c), although the amplitude of w' starts to vary from the bottom of the domain, the maximum w' still occurs within the initial shear layer where $z = -1 \sim 1$. At $J = 1.0$ where the 'RB' completely dominates, w' shows strong propagative features as the magnitude of phase is larger than the magnitude of amplitude.

Figure 8 shows the calculated eigenfunctions for the buoyancy flux perturbation $B' = b'w'$ at $\tilde{\alpha}_{cr} = 0.5$ and $J_b/J = 3$ but with three typical J corresponding to figures 6 and 7. At $J = 0.1$, the buoyancy flux perturbation is formed on the initial shear layer at the center of the domain. As J increases to 0.2, significant differences are found between the 'SS' and 'RB' modes. For the 'RB' mode, as shown in figure 8(b), strong buoyancy flux perturbation occurs near the interface at $z = -2$, with intense and positive magnitude of amplitude compared to figure 8(a). For the 'SS' mode as shown in figure 8(c), although the variations of B' occur mainly in the initial shear layer, such variations appear very weak as the magnitude of the amplitude and phase significantly decrease compared to figure 8(a) and 8(b). At $J = 1.0$, the buoyancy flux perturbations are almost negligible. The transitional behaviors of B' from the 'SS' mode to the 'RB' mode suggests that as unstable stratification increases, the buoyancy flux generated from the bottom thermal boundary will gradually smooth out the buoyancy flux perturbations generated by the central shear stratified layer and eventially dominates in the entire domain.

CONCLUSIONS

The influences of the bottom thermal convection region, in terms of an unstable stratification factor J_b, are added to the Taylor-Goldstein equations to describe the stability features of the sheared convective boundary layer (SCBL) flow. As J_b is introduced into the Taylor-Goldstein equation system, new unstable regions indicating thermal instability are found above the critical stratification factor $J = 0.25$, for the shear stratified flow, in the $J - \tilde{\alpha}$ plane, in addition to the semicircle instability region of the classic sheared stratified flow at $J < 0.25$. As the stratification ratio J_b/J further increases, the thermal unstable region expands and gradually merges with the shear stratified unstable regions. In the $J \sim \tilde{\sigma}$ and $\tilde{\alpha} \sim \tilde{\sigma}$ planes, increasing J_b expands the thermal unstable regions and accordingly leads to domination of the thermal unstable mode over the shear stratified unstable mode. It is further found that the temporal growth rate of the thermal unstable mode increases in a parabolic fashion with the stratification ratio J_b/J and gradually approaches, intersects and at last overwhelms the temporal growth rate of the shear stratified mode, leading to a transition from shear stratified dominant SCBL mode to thermal convection dominant SCBL mode. The critical transition condition for SCBL flow is found at $J_b/J = 3$ and $\tilde{\alpha} = 0.5$. The analysis of the eigenfunctions of the buoyancy perturbation b', vertical velocity perturbation w' and buoyancy flux perturbation $B' = b'w'$ shows distinctively different spatial perturbation structures for the shear stratified dominant mode, transitional mode and the thermal dominant mode.

ACKNOWLEDGEMENT

The support from the Australian Research Council is gratefully acknowledged. Y. Xiao also would like to thank James Cook University for the JCUPRS scholarship.

REFERENCES

Drazin, P. G. & Reid, W. H. 2004 *Hydrodynamic Stability*, 2nd edn. Cambridge University Press.

Hazel, P. 1972 Numerical studies of the stability of inviscid stratified shear flows. *Journal of Fluid Mechanics* **51**, 39–61.

Liu, Z., Thorpe, S. A. & Smyth, W. D. 2012 Instability and hydraulics of turbulent stratified shear flows. *Journal of Fluid Mechanics* **695**, 235–256.

Moler, C. B. & Stewart, G. W. 1973 An algorithm for generalzied matrix eigenvalue problems. *SIAM Journal on Numerical Analysis* **10**, 241–256.

Raasch, S. & Franke, T. 2011 Structure and formation of dust devil-like vortices in the atmospheric boundary layer: A high-resolution numerical study. *Journal of Geophysical Research* **116**, D16120.

Smyth, W. D., Moum, D. J. & Nash, J. D. 2011 Narrowband, high-frequency oscillations at the equator. part ii: Properties of shear instabilities. *Journal of Physical Oceanography* **41**, 412–428.

Stewart, N., Holmes, D. & Lin, W. 2014 Direct numerical simulation of sheared convective boundary layer mixing and entrainment. In *Proceedings of 19th Australasian Fluid Mechanics Conference*. Melbourne, Australia.

Sun, W. 1976 Linear stability of penetrative convection. *Journal of the Atmospheric Sciences* **33**, 1911–1920.

Thorpe, S. A., Smyth, W. D. & Li, L. 2013 The effect of small viscosity and diffusivity on the marginal stability of stably stratified shear flows. *Journal of Fluid Mechanics* **731**, 461–476.

Whitehead, J. A. & Chen, M. M. 1972 Thermal instability and convection of a thin fluid layer bounded by a stable stratification. *Journal of Fluid Mechanics* **40**, 549–576.

Yang, D., Hu, L. H., Hou, R., Jiang, Y. Q., Liu, S. & Tang, F. 2010 Experimental study on buoyant flow stratification induced by a fire in a horizontal channel. *Applied Thermal Engineering* **30**, 872–878.